SIGNAL-DEPENDENT NOISE REMOVAL IN POINTWISE SHAPE-ADAPTIVE DCT DOMAIN WITH LOCALLY ADAPTIVE VARIANCE

Alessandro Foi, Vladimir Katkovnik, and Karen Egiazarian

Institute of Signal Processing, Tampere University of Technology
P.O. Box 553, 33101, Tampere, Finland
web: www.cs.tut.fi/~foi email: firstname.lastname@tut.fi

ABSTRACT

This paper presents a novel effective method for denoising of images corrupted by signal-dependent noise. Denoising is performed by coefficient shrinkage in the shape-adaptive DCT (SA-DCT) transform-domain. The Anisotropic Local Polynomial Approximation (LPA) - Intersection of Confidence Intervals (ICI) technique is used to define the shape of the transform's support in a pointwise adaptive manner. The use of such an adaptive transform support enables both a simpler modelling of the noise in the transform domain and a sparser decomposition of the signal. Consequently, coefficient shrinkage is very effective and the reconstructed estimate's quality is high, in terms of both numerical error-criteria and visual appearance, with sharp detail preservation and clean edges. Simulation experiments demonstrate the superior performance of the proposed algorithm for a wide class of noise models with a signal-dependent variance, including Poissonian (photon-limited imaging), film-grain, and speckle noise.

1. INTRODUCTION

In many applications the observed signal is corrupted by a signal-dependent noise. The most widely encountered models are Poisson, film-grain, multiplicative, and speckle noise. Their common feature is that the variance of the noise is directly related to the true-signal's intensity. In particular, because of the inherent "photon-counting" process within digital imaging sensors, the noise found in digital images is signal-dependent, with brighter parts of the image having a larger noise variance, and typically following a Poissonian distribution.

Starting with classical filters, such as those by Lee, Kuan, and Frost, a number of adaptive approaches for signal-dependent noise removal have been developed and proposed, in spatial (e.g., [7], [13], [2]) as well as in transform domain (e.g., [15], [16], [12], [3]).

In this paper we present a novel effective transform-based method for denoising of images corrupted by signal-dependent noise. Denoising is performed by coefficient shrinkage in the Shape-Adaptive DCT (SA-DCT) [14] transform-domain. The Anisotropic Local Polynomial Approximation (LPA) - Intersection of Confidence Intervals (ICI) technique [10, 9] is used to define the shape of the transform's support in a pointwise adaptive manner. On such adaptive supports the signal is smooth and nearly constant, allowing for a simpler modelling of the noise within each transform support and enabling a sparser decomposition of the signal in the transform domain. Thus, coefficient shrinkage (e.g., hard-thresholding and Wiener filtering) can be employed directly, accurately, and very effectively. As a result, the reconstructed estimate's quality is high, in terms of both numerical error-criteria and visual appearance. In particular, thanks to shape-adaptive transform supports, the estimates exhibit sharp detail preservation and clean edges.

This work was supported by the Finnish Funding Agency for Technology and Innovation (Tekes), AVIPA2 project, and by the Academy of Finland, project No. 213462 (Finnish Centre of Excellence program 2006 - 2011).

The key element of our approach to signal-dependent noise is the use of a locally adaptive estimate of the noise variance, an estimate which is progressively refined during the various stages of the algorithm. The presented method generalizes and extends both the Pointwise SA-DCT filter [4] (originally developed for denoising of additive white Gaussian noise (AWGN)) and the Adaptive-Size Block-DCT (AS B-DCT) algorithm [3] (for signal-dependent noise removal with adaptive-size block transforms), recently proposed by authors.

The rest of the paper is organized as follows. In the next section we introduce the general signal-dependent noise model and the notation used throughout the paper. The algorithm is then presented in detail: construction of the adaptive-shape support, hard-thresholding in SA-DCT-domain, aggregation of overlapping local estimates, and empirical Wiener filtering in SA-DCT domain. The last section is devoted to experimental results for removal of Poissonian (photon-limited imaging), film-grain, and speckle noises.

2. PRELIMINARIES

2.1 Signal-dependent noise model

We consider observations $z(x)$, $x \in X \subset \mathbb{Z}^2$, with the expectations $E\{z(x)\} = y(x) \geq 0$, where the errors (noise) $\eta(x) = z(x) - y(x)$ are independent and the variance of these observations is modeled as

$$\sigma_z^2(x) = var\{z(x)\} = var\{\eta(x)\} = \rho(y(x)), \qquad (1)$$

ρ being a given positive function of y called the *variance function*. For example, $\rho(y) = y$, $\rho(y) = y^2$, and $\rho(y) = \left(Ky^{\alpha}\right)^2$ for the Poisson, gamma, and film-grain observation models, respectively.

The problem is to reconstruct the true image y from the noisy observations z.

2.2 Shape-Adaptive DCT transform and notation

The SA-DCT [14] is computed by cascaded application of one dimensional varying-length DCT transforms first on the columns and then on the rows that constitute the considered region. In our implementation, we use the orthonormal SA-DCT transform (obtained using orthonormal 1-D DCT transforms) with mean (i.e., DC) separation [11].

We denote by $T_U : \mathcal{U} \to \mathcal{V}_U$ the orthonormal SA-DCT transform obtained for a region $U \subset X$, where $\mathcal{U} = \{g : U \to \mathbb{R}\}$ and $\mathcal{V}_U = \{\varphi : V_U \to \mathbb{R}\}$ are function spaces and $V_U \subset \mathbb{Z}^2$ indicates the domain of the transform coefficients. Let $T_U^{-1} : \mathcal{V}_U \to \mathcal{U}$ be the inverse transform of T_U.

Given a function $f : X \to \mathbb{R}$, a subset $U \subset X$, and a function $g : U \to \mathbb{R}$, we denote by $f_{|U} : U \to \mathbb{R}$ the restriction of f on U, $f_{|U}(x) = f(x)\ \forall x \in U$, and by $g^{|X} : X \to \mathbb{R}$ the zero-extension of g to X, $\left(g^{|X}\right)_{|U} = g$ and $g^{|X}(x) = 0\ \forall x \in X \setminus U$. The characteristic (indicator) function of U is defined as $\chi_U = 1_{|U}{}^{|X}$. We denote by $|U|$ the cardinality (i.e. the number of its elements) of U. The

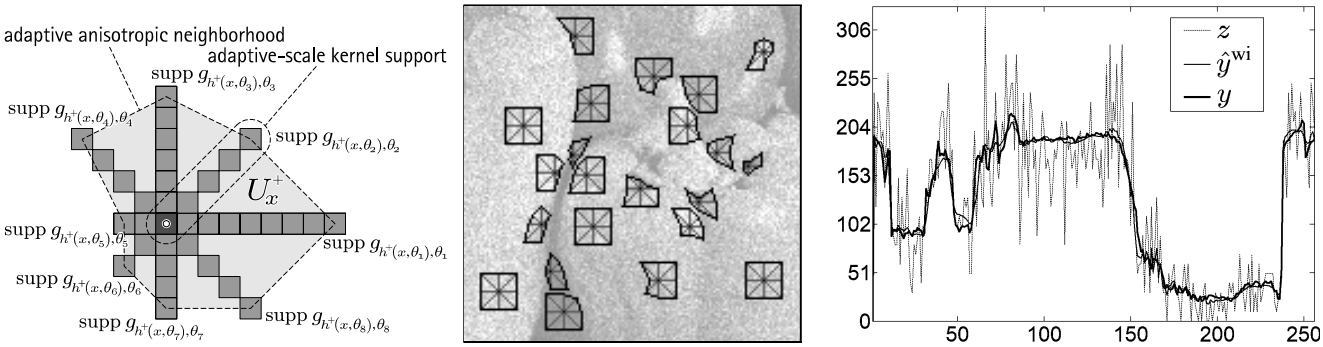

Figure 1: LPA-ICI anisotropic neighborhoods. One-dimensional directional LPA kernels are used for 8 directions. The anisotropic neighborhood U_x^+ is constructed as the polygonal hull of the adaptive-scale kernels' supports (left). Some examples of the anisotropic neighborhoods $\tilde{U}_x^+$ used for SA-DCT filtering of the *Peppers* image (middle) corrupted by Poissonian noise (χ=0.1). The plot on the right shows cross-sections (column 87) of the true image y, of the noisy observation z, and of the Pointwise SA-DCT estimate $\hat{y}^{\mathrm{wi}}$. The signal-dependent nature of the noise is clearly visible.

mean value of f on U is $m_U(f) = \frac{1}{|U|}\sum_{x\in U} f(x)$. The symbol "$\circledast$" stands for the convolution operation.

3. ALGORITHM

The overall algorithm comprises two stages. The first stage (Sections 3.1.1-3.1.3) is based on hard-thresholding. The second stage (Sections 3.2.1-3.2.3) is based on empirical Wiener filtering, using the hard-thresholding estimate obtained in Section 3.1.3 as a reference estimate.

The first step in each stage employs the Anisotropic LPA-ICI technique [10, 9] in order to identify adaptive neighborhoods where the image can be assumed to be locally smooth (polynomial fit) and nearly constant.

3.1 Stage 1: Hard-thresholding in Pointwise SA-DCT domain

3.1.1 Adaptive-shape neighborhood

We initialize the algorithm with a simple, rough estimate $\hat{\sigma}_z^2$ of the variance σ_z^2 obtained as the variance function evaluated on the noisy data, $\hat{\sigma}_z^2 = \rho(|z|)$.

For every specified direction θ_k, $k = 1,\dots,K$, a varying-scale family of 1-D directional-LPA convolution kernels $\{g_{h,\theta_k}\}_{h\in H}$ is used to obtain a corresponding set of directional varying-scale estimates $\{\hat{y}_{h,\theta_k}\}_{h\in H}$, $\hat{y}_{h,\theta_k} = z \circledast g_{h,\theta_k}$, $h \in H$, where $H \subset \mathbb{R}^+$ is the set of scales. For these 1-D kernels, the length of the support coincides with the value of the scale. The pointwise standard-deviations of the estimates $\hat{y}_{h,\theta_k}$ are estimated as $\hat{\sigma}_{\hat{y}_{h,\theta_k}} = \sqrt{\hat{\sigma}_z^2 \circledast g_{h,\theta_k}^2}$, $h \in H$. Thus, for each point (pixel) $x \in X$ we obtain a sequence of confidence intervals $\left\{\left[\hat{y}_{h,\theta_k}(x) - \Gamma\hat{\sigma}_{\hat{y}_{h,\theta_k}}(x), \hat{y}_{h,\theta_k}(x) + \Gamma\hat{\sigma}_{\hat{y}_{h,\theta_k}}(x)\right]\right\}_{h\in H}$, where Γ is a positive threshold parameter. These intervals are then compared according to the ICI rule [6, 8], and as a result an adaptive scale $h^+(x,\theta_k) \in H$ is defined for every $x \in X$. Precisely, the adaptive $h^+(x,\theta_k)$ is defined as the largest scale h such that the intersection of all confidence intervals corresponding to scales smaller than h is non-empty. The procedure is repeated for all specified directions. Thus, for a fixed $x \in X$ we have K directional adaptive scales $h^+(x,\theta_k)$, $k = 1,\dots,K$.

In our implementation, we use $K = 8$ directions and construct the adaptive neighborhood $\tilde{U}_x^+$ of x as $\tilde{U}_x^+ = \left\{v \in X : (x - v) \in U_x^+\right\}$, where U_x^+ is the polygonal hull of the supports of the adaptive-scale kernels $\left\{g_{h^+(x,\theta_k),\theta_k}\right\}_{k=1}^{8}$. Figure 1 illustrates (left) how the neighborhood U_x^+ is constructed and shows (middle) some examples of these neighborhoods for a noisy image corrupted by Poissonian noise. Observe how these neighborhoods adapt to edges and variations in the image intensity and that in each neighborhood the underlying image is smooth and nearly constant.

3.1.2 Hard-thresholding in SA-DCT domain: local estimates

For every neighborhood $\tilde{U}_x^+$, $x \in X$, we construct a *local* estimate $\hat{y}_{\tilde{U}_x^+} : \tilde{U}_x^+ \to \mathbb{R}$ of the signal y by hard-thresholding in SA-DCT domain.

The typically encountered variance functions ρ, such as those mentioned in Section 2.1, are smooth functions of their argument y. As a consequence, on neighborhoods where the signal is nearly constant, so is its variance. It means that with a good approximation, the variance can be assumed to be constant when the transform's support is restricted to a region of signal uniformity such as the adaptive neighborhood $\tilde{U}_x^+$. Thus, locally, the hard-thresholding can be performed as in the standard case [4] where the variance is everywhere constant, provided that a locally adaptive estimate $\hat{\sigma}_z^2\left(\tilde{U}_x^+\right)$ of the variance of the noise in $\tilde{U}_x^+$ is used.

Such a locally adaptive $\hat{\sigma}_z^2\left(\tilde{U}_x^+\right)$ can be obtained from the mean $m_{\tilde{U}_x^+}(z)$ through the variance function as $\hat{\sigma}_z^2\left(\tilde{U}_x^+\right) = \rho\left(\left|m_{\tilde{U}_x^+}(z)\right|\right)$. For any given neighborhood $\tilde{U}_x^+$, this adaptive variance is a constant. Hence, the local estimate $\hat{y}_{\tilde{U}_x^+}$ is calculated as

$$\hat{y}_{\tilde{U}_x^+} = T_{\tilde{U}_x^+}^{-1}\left(\Upsilon_x\left(T_{\tilde{U}_x^+}\left(z_{|\tilde{U}_x^+} - m_{\tilde{U}_x^+}(z)\right)\right)\right) + m_{\tilde{U}_x^+}(z), \quad (2)$$

where Υ_x is a hard-thresholding operator based on the threshold

$$\sqrt{\hat{\sigma}_z^2\left(\tilde{U}_x^+\right)\left(2\ln|\tilde{U}_x^+| + 1\right)}. \quad (3)$$

This threshold is essentially Donoho's "universal" threshold using the locally adaptive variance estimate $\hat{\sigma}_z^2\left(\tilde{U}_x^+\right)$.

3.1.3 Global estimate as aggregation of local estimates

The Anisotropic LPA-ICI provides an adaptive neighborhood $\tilde{U}_x^+$ for every $x \in X$. Neighborhoods corresponding to adjacent points are usually overlapping, thus the local estimates $\left\{\hat{y}_{\tilde{U}_x^+}\right\}_{x\in X}$ (2) constitute an overcomplete representation of the image. In order to obtain a single *global* estimate $\hat{y} : X \to \mathbb{R}$ defined on the whole image domain, all the local estimates (2) are averaged together using adaptive weights $w_x \in \mathbb{R}$ in the following convex combination:

$$\hat{y} = \frac{\sum_{x\in X} w_x \hat{y}_{\tilde{U}_x^+}|^X}{\sum_{x\in X} w_x \chi_{\tilde{U}_x^+}}. \quad (4)$$

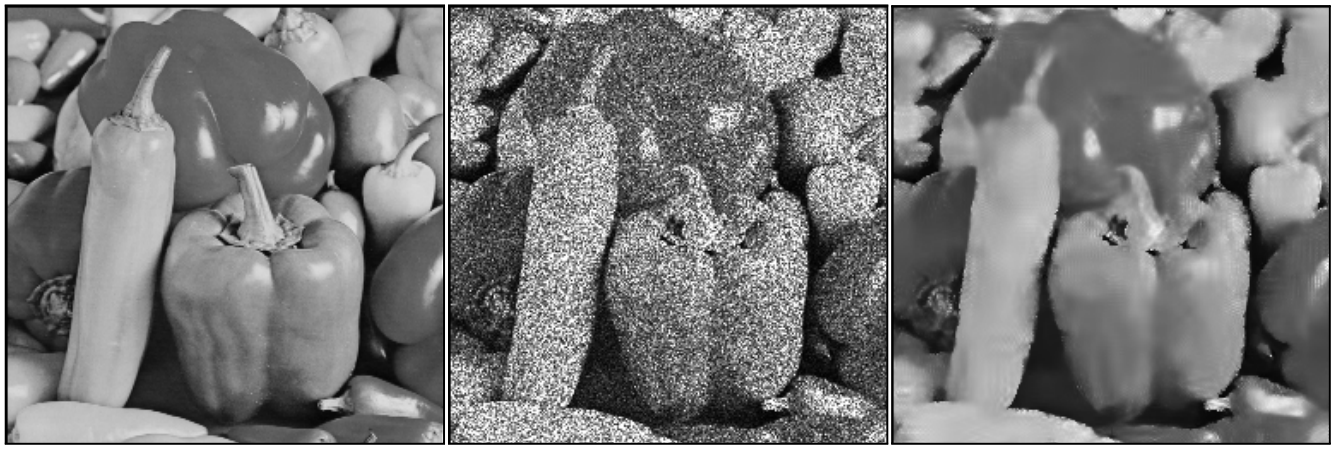

Figure 2: *Peppers* image: (from left to right) original image, noisy observation corrupted by speckle noise (MSE=4442, PSNR=11.6dB), and Pointwise Shape-Adaptive DCT estimate $\hat{y}^{\mathrm{wi}}$ (MSE=193, PSNR=25.3dB).

Figure 3: *Aerial* image: (from left to right) original image, noisy observation corrupted by film-grain noise (MSE=829, PSNR=18.9dB), and Pointwise Shape-Adaptive DCT estimate $\hat{y}^{\mathrm{wi}}$ (MSE=142, PSNR=26.6dB).

Analogously to [4], the weights w_x depend on the total sample variance of $\hat{y}_{\tilde{U}_x^+}$–thus, on the number N_x^{har} of non-zero coefficients after thresholding and on the local variance $\hat{\sigma}_z^2\left(\tilde{U}_x^+\right)$–and on the size of the neighborhood $|\tilde{U}_x^+|$:

$$w_x = \frac{\hat{\sigma}_z^{-2}\left(\tilde{U}_x^+\right)}{\left(1+N_x^{\mathrm{har}}\right)|\tilde{U}_x^+|}. \tag{5}$$

3.2 Stage 2: Wiener filtering in Pointwise SA-DCT domain

3.2.1 Improved adaptive-shape neighborhood

The estimate of the variance $\hat{\sigma}_z^2$ used in Section 3.1.1 (calculated from z through the variance function ρ) is indeed rough. A better estimate $\hat{\sigma}_z^2$ can now be calculated from the above $\hat{y}$ as $\hat{\sigma}_z^2 = \rho\left(|\hat{y}|\right)$. The Anisotropic LPA-ICI approach is used once more to deliver more accurate adaptive scales. We modify slightly the procedure from Section 3.1.1, in that the LPA estimates $\{\hat{y}_{h,\theta_k}\}_{h\in H}$ are now calculated not from z but from $\hat{y}$ (4), as the convolution $\hat{y}_{h,\theta_k} = \hat{y} \circledast g_{h,\theta_k}$, $h \in H$. The standard-deviations needed for the construction of the confidence intervals are calculated again as $\hat{\sigma}_{\hat{y}_{h,\theta_k}} = \sqrt{\hat{\sigma}_z^2 \circledast g_{h,\theta_k}^2}$, $h \in H$, with $\hat{\sigma}_z^2 = \rho\left(|\hat{y}|\right)$. As a result of the ICI rule, we obtain, for each $x \in X$, the new directional adaptive scales $h^+(x,\theta_k)$, $k = 1,\ldots,K$, and thus the corresponding adaptive-shape neighborhood $\tilde{U}_x^+$.

3.2.2 Wiener filtering in SA-DCT domain: local estimates

Using the estimate $\hat{y}$ (4), the empirical Wiener filter in the SA-DCT domain works as follows. For a fixed x, let $\varphi_{z,x} : V_{\tilde{U}_x^+} \to \mathbb{R}$ and $\varphi_{\hat{y},x} : V_{\tilde{U}_x^+} \to \mathbb{R}$ be, respectively, the SA-DCT (on $\tilde{U}_x^+$) coefficient of z and $\hat{y}$, calculated as

$$\varphi_{z,x} = T_{\tilde{U}_x^+}\left(z_{|\tilde{U}_x^+} - m_{\tilde{U}_x^+}(z)\right), \tag{6}$$

$$\varphi_{\hat{y},x} = T_{\tilde{U}_x^+}\left(\hat{y}_{|\tilde{U}_x^+} - m_{\tilde{U}_x^+}(z)\right), \tag{7}$$

where the mean $m_{\tilde{U}_x^+}(z)$ of z is subtracted before applying the transform. The *local* Wiener estimate $\hat{y}^{\mathrm{wi}}_{\tilde{U}_x^+}$ is defined as

$$\hat{y}^{\mathrm{wi}}_{\tilde{U}_x^+} = T^{-1}_{\tilde{U}_x^+}\left(\omega_x \varphi_{z,x}\right) + \varpi_x m_{\tilde{U}_x^+}(z), \tag{8}$$

where $\omega_x \in \mathcal{V}_{\tilde{U}_x^+}$ and $\varpi_x \in \mathbb{R}$ are respectively the Wiener attenuation factors for $\varphi_{z,x}$ and for the subtracted mean value $m_{\tilde{U}_x^+}(z)$,

$$\omega_x = \frac{\varphi^2_{\hat{y},x}}{\varphi^2_{\hat{y},x} + \sigma_x^2}, \qquad \varpi_x = \frac{m^2_{\tilde{U}_x^+}(\hat{y})}{m^2_{\tilde{U}_x^+}(\hat{y}) + \hat{\sigma}_z^2\left(\tilde{U}_x^+\right)/|\tilde{U}_x^+|}, \tag{9}$$

and $\hat{\sigma}_z^2\left(\tilde{U}_x^+\right)$ is a local adaptive estimate of the variance of z in $\tilde{U}_x^+$ calculated as $\rho\left(\left|m_{\tilde{U}_x^+}(\hat{y})\right|\right)$.

Figure 4: *Cameraman* image: (from left to right) original image, noisy observation corrupted by Poissonian noise ($\chi = 30/255$, MSE=1015, PSNR=18.1dB), and Pointwise Shape-Adaptive DCT estimate $\hat{y}^{\mathrm{wi}}$ (MSE=100, PSNR=28.1dB).

Figure 5: *Cameraman* image: (from left to right) noisy observation corrupted by Poissonian noise ($\chi = 60/255$, MSE=504, PSNR=18.1dB), AS B-DCT estimate [3] (MSE=70, PSNR=29.7dB), and Pointwise Shape-Adaptive DCT estimate $\hat{y}^{\mathrm{wi}}$ (MSE=68, PSNR=29.8dB).

3.2.3 Final global estimate as aggregation of local estimates

The *global* estimate $\hat{y}^{\mathrm{wi}}$ can be obtained analogously as in (4), using the convex combination with the adaptive weights w_x^{wi}:

$$\hat{y}^{\mathrm{wi}} = \frac{\sum_{x \in X} w_x^{\mathrm{wi}} \hat{y}^{\mathrm{wi}}_{\tilde{U}_x^+ | X}}{\sum_{x \in X} w_x^{\mathrm{wi}} \chi_{\tilde{U}_x^+}}, \quad w_x^{\mathrm{wi}} = \frac{\hat{\sigma}_z^{-2}\left(\tilde{U}_x^+\right)}{\left(\varpi_x^2 + \sum_{V_{\tilde{U}_x^+}} \omega_x^2\right) |\tilde{U}_x^+|}. \quad (10)$$

Similarly to (5), the term $\hat{\sigma}_z^2\left(\tilde{U}_x^+\right)\left(\varpi_x^2 + \sum_{V_{\tilde{U}_x^+}} \omega_x^2\right)$ in the adaptive weights corresponds to an estimate of the total sample variance of $\hat{y}^{\mathrm{wi}}_{\tilde{U}_x^+}$.

The Pointwise SA-DCT results which we present in this paper correspond to the $\hat{y}^{\mathrm{wi}}$ estimate (10).

3.3 Complexity

The presented method for signal-dependent noise removal inherits the same low computational complexity of the standard Pointwise SA-DCT developed for AWGN (we refer the reader to [4] for a detailed analysis of the computational complexity of the standard Pointwise SA-DCT algorithm). In fact, the extra operations in this generalized algorithm are essentially only the convolutions needed to calculate $\hat{\sigma}_{\hat{y}_{h,\theta_k}}$, and the Anisotropic LPA-ICI in the second stage of the algorithm. Both are computationally negligible compared to the multiple forward and inverse SA-DCT transforms performed in Sections 3.1.2 and 3.2.2. The locally adaptive variance estimates $\hat{\sigma}_z^2\left(\tilde{U}_x^+\right)$ are also calculated "almost for free", since the local means $m_{\tilde{U}_x^+}(z)$ and $m_{\tilde{U}_x^+}(\hat{y})$ are anyway required by standard algorithm for AWGN.

4. EXPERIMENTAL RESULTS

We show experimental results for three common types of signal-dependent noise: the "scaled" *Poisson* noise, $\chi z \sim \mathcal{P}(\chi y)$, $\chi \in \mathbb{R}^+$, the *film-grain* noise, $z = y + Ky^{\alpha}\eta$, $K, \alpha \in \mathbb{R}^+$ and $\eta \sim \mathcal{N}(0,1)$, and the "multiple-look" *speckle* noise, $z = L^{-1}\sum_{i=1}^{L} y\epsilon_i$, $\epsilon_i \sim \mathcal{E}(\beta)$, $\beta \in \mathbb{R}^+$. The calligraphic letters $\mathcal{P}$, $\mathcal{N}$, and $\mathcal{E}$ denote, respectively, the Poisson, Gaussian, and exponential distributions. For the above observation models, the variance functions $\rho(y) = \sigma_z^2$ are $\rho(y) = y/\chi$, $\rho(y) = K^2 y^{2\alpha}$, and $\rho(y) = y^2\beta/L$, respectively. The true signal y is assumed to have range [0,255].

Firstly, in Table 1 we give a comparison for the simulations presented in [13] for the above noise models with parameters χ=0.1, K=3.3, α=0.5, L=4, and β=1. In the table our results are compared against the adaptive-neighborhood filter [13], the noise-updating repeated Wiener filter [7] (as quoted in [13]), the recursive anisotropic LPA-ICI technique [2, 5], and the AS B-DCT algorithm [3].

Next, in Table 2 we compare our results for removal of Poissonian noise ($\chi = \frac{30}{255}, \frac{60}{255}, \frac{90}{255}, \frac{120}{255}$) against those obtained by two other transform-based methods [15],[12] recently developed specifically for this type of noise, by the recursive anisotropic LPA-ICI technique, and by the AS B-DCT algorithm.

	noise type	noisy	[7]	[13]	[2, 5]	[3]	P. SA-DCT
Peppers	*Poisson* (χ=0.1)	1243	160	145	120	104	**95**
	Film-grain	1351	169	150	123	109	**97**
	Speckle	4442	372	378	286	225	**193**
Aerial	*Poisson* (χ=0.1)	758	252	179	183	149	**141**
	Film-grain	829	267	188	185	154	**142**
	Speckle	1698	387	318	330	257	**242**

Table 1: *MSE* results for different noise types and denoising algorithms.

	χ	noisy	[15]	[12]	[2, 5]	[3]	P. SA-DCT
Lena	*30/255*	1054	168	143	73	61	**55**
	60/255	525	117	96	50	42	**38**
	90/255	349	93	75	40	34	**31**
	120/255	262	81	63	34	30	**27**
Cameraman	*30/255*	1015	199	154	136	107	**100**
	60/255	504	140	97	89	70	**68**
	90/255	336	113	74	70	55	**53**
	120/255	254	97	61	60	46	**45**

Table 2: *MSE* comparison against algorithms for Poissonian noise.

The results in the tables show that the proposed algorithm outperforms all other methods, for all considered noise models and noise levels. In terms of MSE, the improvement is significant especially for higher noise.

Figures 2, 3, and 4 provide a demonstration of the visual quality of the proposed Pointwise SA-DCT technique. Edges and small details are restored quite sharply, with very few noticeable artifacts. Figure 5 presents a comparison between denoised estimates obtained by the AS B-DCT and by the Pointwise SA-DCT algorithms. Although the numerical difference is marginal, the two estimates are visually quite different. The AS B-DCT estimate has visible artifacts in the vicinity of sharp edges, and especially along the diagonal ones; the Pointwise SA-DCT estimate presents instead clean-cut edges that are comparable with those of the original image (shown in Figure 4(left)), thanks to superior spatial adaptivity.

We conclude remarking that the proposed method based on locally adaptive variance estimates is superior to the simpler approach where the noisy observations are preprocessed by a non-linear variance-stabilizing transformation and then filtered by an algorithm for AWGN. In particular, let us consider the Poissonian noise case and the procedure where the Anscombe transformation [1] is employed to stabilize the variance and denoising is then performed by the Pointwise SA-DCT algorithm [4] for AWGN, followed by inverse Anscombe transformation. For this simpler approach the MSE results are as follows: $\chi = 0.1$ *Peppers* MSE=103, *Aerial* MSE=153; $\chi = 30/255$ *Lena* MSE=59, *Cameraman* MSE=105. A comparison with the Tables 1 and 2 shows the improvement achieved by the use of locally adaptive variances.

REFERENCES

[1] Anscombe, F.J., "The Transformation of Poisson, Binomial and Negative-Binomial Data", *Biometrika*, vol. 35, no. 3/4, pp. 246-254, 1948.

[2] Foi, A., R. Bilcu, V. Katkovnik, and K. Egiazarian, "Anisotropic local approximations for pointwise adaptive signal-dependent noise removal", *Proc. of XIII European Signal Proc. Conf., EUSIPCO 2005*, Antalya, September 2005.

[3] Foi, A., R. Bilcu, V. Katkovnik, and K. Egiazarian, "Adaptive-Size Block Transforms for Signal-Dependent Noise Removal", *Proc. 7th Nordic Signal Processing Symposium, NORSIG 2006*, Reykjavik, Iceland, June 2006.

[4] Foi, A., V. Katkovnik, and K. Egiazarian, "Pointwise Shape-Adaptive DCT for High-Quality Denoising and Deblocking of Grayscale and Color Images", *IEEE Trans. Image Process.*, vol. 16, no. 5, pp. 1395-1411, May 2007.

[5] Foi, A., D. Paliy, V. Katkovnik, and K. Egiazarian, "Anisotropic nonparametric image restoration demobox" (MATLAB software), *LASIP (Local Approximations in Signal and Image Processing) Project*, `http://www.cs.tut.fi/~lasip/` , 2005.

[6] Goldenshluger, A., and A. Nemirovski, "On spatial adaptive estimation of nonparametric regression", *Math. Meth. Statistics*, vol. 6, pp. 135-170, 1997.

[7] Jiang, S.S., and A.A. Sawchuk, "Noise updating repeated Wiener filter and other adaptive noise smoothing filters using local image statistics", *Appl. Opt.*, vol. 25, pp. 2326-2337, 1986.

[8] Katkovnik V., "A new method for varying adaptive bandwidth selection", *IEEE Trans. on Signal Proc.,* vol. 47, no. 9, pp. 2567-2571, 1999.

[9] Katkovnik, V., K. Egiazarian, and J. Astola, *Local Approximation Techniques in Signal and Image Processing*, SPIE Press, Monograph vol. PM157, September 2006.

[10] Katkovnik, V., A. Foi, K. Egiazarian, and J. Astola, "Directional varying scale approximations for anisotropic signal processing", *Proc. XII Eur. Signal Process. Conf., EUSIPCO 2004,* pp. 101-104, Vienna, Sep. 2004.

[11] Kauff, P., and K. Schuur, "Shape-adaptive DCT with block-based DC separation and ΔDC correction", *IEEE Trans. Circuits Syst. Video Technol.*, vol. 8, no. 3, pp. 237-242, 1998.

[12] Lu, H., Y. Kim, and J.M.M. Anderson, "Improved Poisson intensity estimation: denoising application using poisson data," *IEEE Trans. Image Process.,* vol. 13, no. 8, pp. 1128-1135, 2004.

[13] Rangarayyan, R.M., M. Ciuc, and F. Faghih, "Adaptive-neighborhood filtering of images corrupted by signal-dependent noise", *Appl. Opt.*, vol. 37, pp. 4477-4487, 1998.

[14] Sikora, T., "Low complexity shape-adaptive DCT for coding of arbitrarily shaped image segments", *Signal Process.: Image Comm.*, vol. 7, pp. 381-395, 1995.

[15] Timmermann, K.E., and R. Nowak, "Multiscale modeling and estimation of Poisson processes with application to photon-limited imaging", *IEEE Trans. Inf. Theory,* vol. 45, no. 3, pp. 846-862, 1999.

[16] Willett, R.M., and R. Nowak, "Platelets: a multiscale approach for recovering edges and surfaces in photon-limited medical imaging", *IEEE Trans. Medical Imaging,* vol. 22, no. 3, pp. 332-350, 2003.